In situ x-ray absorption studies of electrochemically induced phase changes in lithium-doped InSb

H. Tostmann
Chemistry Department, University of Florida, Gainesville, Florida 32611

A. J. Kropf,* C. S. Johnson, J. T. Vaughey, and M. M. Thackeray
Chemical Technology Division, Argonne National Laboratory, Argonne, Illinois 60439
(Received 3 July 2001; revised manuscript received 2 May 2002; published 18 July 2002)

We report a comprehensive analysis of *in situ* x-ray absorption spectroscopy data that provide detailed information about phase transformations of the III-V semiconductor InSb, induced by electrochemical insertion of Li and extrusion of indium. Upon discharging a Li/InSb cell, In is extruded from the zinc-blende-type InSb structure and replaced by Li. Although more than 90% of the In is displaced from the structure, the Sb fcc sublattice remains stable at all degrees of lithiation. This process is reversible. However, in the fully charged state, about 40% of the In remains outside the matrix as In metal, leaving a corresponding number of Schottky vacancies in a $In_{1-y}Sb$ defect structure. The discussion of this paper focuses on the ease and reversibility of the phase changes in InSb electrodes, which is attributed to the stability of the Sb fcc sublattice at all states of discharge and charge, to the lattice compatibility of the different phases, and to the absence of significant charge gradients.

DOI: 10.1103/PhysRevB.66.014106 PACS number(s): 61.43.Dq, 61.72.Vv, 82.45.−h

I. INTRODUCTION

Intercalation of alkali metals into graphite is one of the most prominent examples of inserting atoms into a host lattice—in this case, exceptionally widely spaced carbon layers.[1] The first intercalation compound, KC_8, was reported as early as 1926.[2] This intriguing property of graphite led to the predominant application of graphite intercalation compounds (GIC's) as electrode materials in electrochemical energy systems.[3] For example, graphite is used as the negative electrode in commercially used lithium-ion batteries where the alkali metal is cycled in and out of the graphite lattice during charge and discharge. There are, however, several drawbacks to using GIC electrodes. Most important, lithiated graphite (LiC_6) is susceptible to lithium plating upon overcharging because the potential of LiC_6 is close to that of elemental lithium.[4]

One approach pursued recently to replace graphite as a host for lithium involves the development of intermetallic ''insertion'' electrodes.[5–9] The mechanism of reversible Li insertion and extraction in these intermetallic electrodes is obviously different from GIC's since intermetallic electrodes do not provide widely spaced layers suitable for intercalation. An important feature of these intermetallic ''insertion'' electrodes is the existence of a stable host sublattice, such as the face-centered-cubic (fcc) lattice provided by Sb in InSb. This host sublattice corresponds to the carbon in graphite electrodes. The second component of the intermetallic electrode, in this case the indium of InSb, is replaced reversibly by lithium. Intermetallic electrodes operate several hundred millivolts above the potential of metallic lithium, thus precluding lithium plating.[10] In addition, intermetallic electrodes provide a higher volumetric capacity than graphite, which is an important parameter for the miniaturization of lithium cells and batteries.[7] There are, however, several fundamental questions that need to be addressed before insertion electrodes can be considered as a serious alternative to GIC electrodes: (i) How does lithium insertion affect the structure of the lattice? (ii) How stable is the host lattice? (iii) What is the nature of the phase transformations on a microscopic level? (iv) Are they accompanied by lattice expansion or charge transfer?

The intermetallic compound InSb is a particularly intriguing example of an ''insertion'' electrode. InSb is a III-V semiconductor that undergoes a transition to the metallic state upon insertion of small amounts of lithium. Electrochemical,[7] thermodynamical,[10] and structural[11] characterizations of this electrode have been reported. Recently, we communicated our initial results of an analysis of the In *K*-edge extended x-ray absorption fine-structure (EXAFS).[12] In this paper, we present a comprehensive analysis of both the In and Sb *K*-edge EXAFS, as well as an analysis of the x-ray absorption near-edge structure (XANES). We focus on the atomic-level mechanism of the phase changes that occur during the electrode reactions. Of particular interest is the stability of the Sb host lattice and the ease and reversibility with which these phase transformations take place. Emphasis is placed on the role of (i) lattice compatibility of the different phases and (ii) charge transfer or the lack thereof in facilitating phase transformations. The first point is probed by EXAFS, while the second point is addressed by XANES; both techniques are considered a subset of x-ray absorption fine-structure (XAFS) spectroscopy.[13] We have employed XAFS to overcome the limitations of gathering precise microstructural information by using x-ray diffraction (XRD) techniques. As opposed to XRD, which relies on the presence of long-range order, XAFS probes the local environment around a selected atom. The InSb electrode material is fabricated by high-energy ball milling to reduce the particle size and minimize kinetic limitations.[6] This drastically reduces the effectiveness of XRD but does not greatly affect XAFS. Also, the presence (or absence) of nascent phases such as

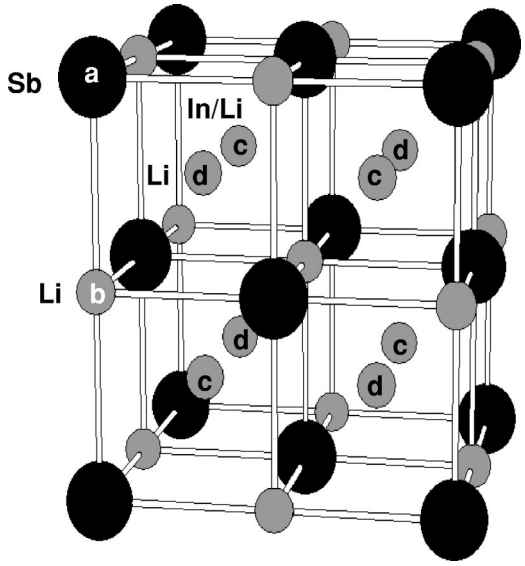

FIG. 1. Schematic representation of the lattices of Sb, InSb, $Li_{x+y}In_{1-y}Sb$, and Li_3Sb as described by a superlattice of a simple ''pseudo'' CsCl unit cell.

metallic In, Li_3Sb, lithiated indium (designated as Li_xIn), and metallic Sb can be detected with XAFS at a significantly lower level and with greater precision than is possible with XRD, which requires that these phases coalesce into a long-ranged periodic array.

An important prerequisite for preserving a stable Sb host lattice during the phase changes that occur as a consequence of Li insertion and In extrusion can be met if the Sb sublattice is compatible with all the phases involved. Figure 1 illustrates how this requirement is satisfied by the InSb electrode. The cubic unit cell shown is a superlattice of a ''pseudo'' CsCl unit cell, obtained by doubling the edges of the CsCl unit cell in three orthogonal directions. The 16 positions of the resulting superlattice can be grouped into four sublattices, each having a fcc structure. For example, if Sb occupies all (a) sites while all other sites remain unoccupied, an Sb fcc host lattice results, which will be of particular importance for the discussion presented below.

If Sb and In occupy their respective (a) and (c) sites, a zinc-blende-type lattice of InSb is formed. The reaction product of a fully lithiated InSb electrode is Li_3Sb, which crystallizes with the Li_3Bi structure, also known as the antitypical Fe_3Al. In terms of the CsCl superlattice, the Li_3Sb structure can be visualized if Li occupies the interstitial sites of InSb [(b) and (d)] and if all the In sites (c) are replaced by Li. No significant structural rearrangement of the Sb sublattice is necessary to accommodate these different phases; a continuous transition between subsequent phases in a $Li_{x+y}In_{1-y}Sb$ system ($0 \leqslant x \leqslant 2; 0 \leqslant y \leqslant 1$) is, therefore, possible if Schottky vacancies are taken into account.

II. EXPERIMENT

The InSb compound was prepared by mechanical alloying (ball milling) of the elements in a stoichiometric ratio in the presence of a solid carbon lubricant. Indium and antimony were purchased from Aldrich (99.99% and 99.995% purity, respectively), and used as received. The product was ground and sieved through a 400-mesh screen to obtain particles smaller than 40 μm in size. The resulting black powder was determined by XRD to be single-phase InSb. Details of the electrode and coin cell preparation are given elsewhere.[7] A small hole was punched in the coin cell and sealed with an epoxy resin to facilitate x-ray beam access to the electrode. The electrolyte was 1-M $LiPF_6$ in 50:50 (w/w%) ethylene carbonate: diethylcarbonate (EC:DEC). The cell therefore has the initial configuration Li/electrolyte/InSb.

The cell was positioned in the x-ray beam with the illuminated area defined by slits (1000 μm vertically, 1500 μm horizontally). The x-ray beam was provided by the undulator beamline of the Materials Research Collaborative Access Team (MRCAT), which is part of the Advanced Photon Source (APS) synchrotron at Argonne National Laboratory, Argonne, IL. This x-ray source is particularly well suited for performing x-ray absorption spectroscopy at high edge energies, as is the case for Sb (30491 eV) and In (27940 eV). By using the Si(333) reflection from a cryogenically cooled double-crystal monochromator, an energy resolution of about 2.5 eV was achieved.[14] The higher-order harmonic content of the beam was attenuated using a platinum-coated mirror, while the fundamental Si(111) reflection was blocked using a 1.5-mm-thick piece of aluminum. The fourth and fifth harmonics of the tapered undulator were used, further reducing the harmonic content of the beam due to mismatching the undulator harmonics and the unwanted Bragg reflections from the monochromator.

To achieve the time resolution necessary to follow the phase transformations in the Li/InSb system while applying a current to the cell, the EXAFS spectra were taken in continuous mode, i.e., with the monochromator moving at a constant speed. This reduces the acquisition time per spectrum to about 6 min by eliminating the time required to step the monochromator. Thus we were able to maintain a constant current in the battery cell at all times and did not have to interrupt the reaction to take a long EXAFS measurement. The potential did not change by more than 0.02 V over a complete spectrum, except during the very beginning of a charge or discharge cycle where the potential changed more rapidly. Data from two experiments are presented. The first data set (cell A) was taken while discharging a freshly prepared cell from its equilibrium potential of 1.5 V down to 0.5 V. The second data set (cell B) is from a ''preconditioned'' cell, for which the initial discharge occurred off-line. The XAFS spectra for cell B were taken while charging from 0.5 to 1.2 V, and then during discharge to 0.1 V. A moderate current density was applied to the cells: 0.3 mA/cm^2 for cell A, 0.4 mA/cm^2 for cell B during charge, and 0.5 mA/cm^2 for cell B during discharge. Current and cell voltage were controlled with a CH Instruments Model 660 potentiostat/galvanostat.[7]

The EXAFS spectra were taken in the fluorescence mode from 150 eV below the edge to 850 eV above the edge. The point density, $\approx$1.2 eV/step, was chosen so that the edge region is defined with a fine enough resolution to allow XANES analysis. The In and Sb *K* edges were scanned al-

TABLE I. Debye-Waller factors for scattering paths used in fitting the EXAFS data (in Å^2); nearest-neighbor (nn) and next-nearest-neighbor (nnn) paths are shown. The first element shown designates the edge for which the path is valid.

path phase	In-Sb (InSb) (nn)	In-In (In) (nn)	In-In (In) (nnn)	In-In (Li_xIn) (nn)	In-Li (Li_xIn) (nnn)	Sb-In (InSb) (nn)	Sb-Sb (InSb) (nnn)	Sb-Li (Li_3Sb) (nn)	Sb-Li (Li_3Sb) (nnn)
	0.0074 ± 0.0012	0.022 ± 0.002	0.037 ± 0.010	0.007 ± 0.002	0.011 ± 0.005	0.0048 ± 0.0011	0.023 ± 0.005	0.013 ± 0.008	0.013 ± 0.010

ternately for the duration of the experiment using a fluorescence detector filled with Kr gas. The edge energy was calibrated using the transmission spectrum of ground single-crystal InSb powder recorded concurrently with each measurement.

III. DATA ANALYSIS

Extended x-ray absorption fine structure refers to the oscillatory structure in the x-ray absorption coefficient as a function of incident photon energy E, $\mu(E)$, just above the x-ray absorption edge. While the position of the edge depends on the type of atom investigated, the oscillations are a condensed matter effect and a signature of the local environment around the selected central atom.[13,15] EXAFS can be visualized as interference effects between photoelectron waves emanating from the central atom and waves backscattered along various paths from surrounding atoms, typically from three to four shells away. To extract the interesting information from these oscillations, such as bond lengths, coordination numbers, and phase fractions, a comprehensive analysis is performed. First, the edge step is normalized to unity, and the slowly varying background, μ_0, is removed, resulting in the EXAFS spectrum $\chi(E)$,

$$\chi(E)=\frac{[\mu(E)-\mu_0(E)]}{\Delta\mu_0}, \tag{1}$$

with the edge-jump normalization factor $\Delta\mu_0$. The EXAFS spectrum is then converted from energy space to k space, where k is the photoelectron wave vector, calculated relative to the edge energy E_0,

$$E-E_0=\frac{\hbar^2k^2}{2m_e}, \tag{2}$$

with m_e being the mass of a free electron. The resulting EXAFS spectrum $\chi(k)$ can be viewed as a sum of the contributing scattering paths i and described mathematically as a sum of individual components,

$$\chi(k)\propto\sum_i S_{0,i}^2N_i\frac{f(k)}{kR^2}\sin[2kR_i+\delta(k)] \times\exp[-2R_i/\lambda(k)]\exp(-2\sigma^2k^2), \tag{3}$$

with the amplitude reduction factor S_0^2, coordination number N, backscattering amplitude $f(k)$, backscattering phase δ, bond length R, mean free path length λ, and Debye-Waller (DW) factor σ^2. The paths, for example the Sb-In nearest neighbor linear scattering path, are obtained from high-order multiple-scattering theory as implemented in the FEFF software package (Version 8.0).[16] Whenever possible, the theoretical calculations were calibrated to experimental references such as Sb metal, In metal, and InSb powder. A physically reasonable combination of scattering paths is then fit to the windowed and k-weighted data in r space using the FEFFIT code.[17]

The number of parameters from Eq. (3) used in the fit (N_i, R_i, and σ_i^2 for each path i) is restricted by the following conditions: The contribution of an individual path is given by N_i, which can be calibrated to the value of the pure component. For example, the reduction of the amplitude of the Sb-In nearest-neighbor path is normalized to N of pure InSb ($N=4$). A reduction of N_{SbIn} and an increase in N_{SbLi} obviously point to a phase reaction in which In neighbors are replaced by Li neighbors. The DW factor, a measure for the degree of structural and thermal disorder, is fixed at the values found for the experimental standards. Where no suitable standard was available, namely, for Li_xIn and Li_3Sb, the DW factor was constrained to the value found for the spectra at which those components dominate the overall EXAFS spectrum. The DW factors used throughout the analysis are compiled in Table I. The DW factors for the In-Sb path (0.0074 ± 0.0012 Å^2) and the Sb-In path (0.0048 ± 0.0011 Å^2) are expected to agree within the error bar, a requirement that is not entirely met. This may be due to a possible separation problem between the In-In metal path and the In-Sb path for the In-edge data. The analysis presented here is not significantly affected by the choice of the DW factor for the In-Sb path. Therefore, we chose to use the value of 0.0074 Å^2 since it reflects the reality of the presence of at least 40% In metal at all times after the conditioning cycle.

The relative contribution of different scattering paths to the overall EXAFS signal is illustrated by a representative example in Fig. 2. The Fourier transform of the k^2-weighted Sb-edge EXAFS spectrum of a lithiated InSb electrode at 1.04 V is shown. The data were taken during the charge cycle for cell B. As will be discussed in more detail below, at a potential of 1.04 V about 50% of the In has been cycled out of the InSb lattice and replaced by Li. This is reflected by the fact that the Sb-In nn path (solid line in the lower half of Fig. 2) is not sufficient to describe the first-shell data centered around 2.8 Å. The presence of Li as a neighbor to Sb is

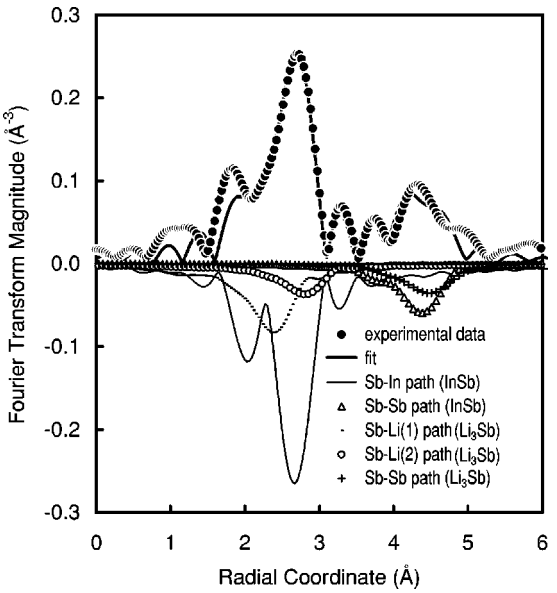

FIG. 2. Fourier transform of the k^2-weighted Sb-edge EXAFS spectrum of a lithiated InSb electrode at 1.04 V during the charging cycle of cell B. Upper half: overall fit of the sum of five scattering paths to the data; lower half: contribution of each scattering path to the EXAFS spectrum. For information about the EXAFS data windows, see the caption of Fig. 4.

represented by the inclusion of two Sb-Li paths taken from the FEFF calculation for Li_3Sb (dotted line and open circles). Lithium occupies two different nn positions in Li_3Sb, and thus, two different paths are used to describe the first-shell data. Two paths describe the second-shell data (centered at around 4.5 Å), one from InSb (open triangles) and one from Li_3Sb (plus symbols).

To analyze the small changes in the electrode near the end points of the charge and discharge cycles, a difference analysis technique has been used to supplement the conventional fitting method. The difference technique was described by Miller *et al.* in the context of *in situ* XAFS measurements of hydrodesulfurization catalysts.[18] It is based on the fact that the fine structure is a linear combination of scattering paths, as in Eq. (3). In experiments, such as a charging battery, where there are only small changes from scan to scan, the effect is to emphasize small coordination environment differences by taking the difference between two data files and analyzing the residual signal. In so doing, one can fit the signal from a path that would otherwise make a negligible contribution to the error function used for minimization in the fitting procedure. This allows a more precise determination of the potential at which the coordination environment changes in a statistically significant manner, as opposed to the effect of random fluctuations in the data that alter the observed fit parameters.

Error analysis is built into the FEFFIT package.[17] For the radial distance and Debye-Waller factor, these are the uncertainties that are quoted. The uncertainties for the coordination number, and thus the phase fractions, are complicated slightly by uncertainty in the amplitude reduction factor S_0^2. Finally, the upper limit to the Sb-Li path contribution at greater than 1.0 V has been determined by evaluating the *R* factor, an indicator used by FEFFIT that measures the difference between the fit and the experimental data, scaled by the amplitude of the data. The criterion used was the amount of Sb-Li added that resulted in doubling the *R* factor, while allowing all free parameters to float. This method generally increased the uncertainty, compared to the typical error analysis.

IV. RESULTS

Two experiments have been performed: First, a freshly prepared Li/InSb coin cell has been discharged to 0.5 V (cell A). Second, a cell that had been discharged to 0.5 V prior to the XAFS experiment has been charged from 0.5 to 1.2 V and again discharged from 1.2 to 0.1 V (cell B). The initial discharge cycle is different from all subsequent cycles since Li is inserted for the first time, leading to irreversible structural changes. Subsequent cycles, however, are predominantly reversible, as shown by long-term electrochemical studies.[7] The charge and discharge cycles of cell B can, therefore, be viewed as representative of the behavior of a Li/InSb cell in operation.

The galvanostatic potential vs. time curve for the conditioning cycle of cell A is shown in Fig. 3(c). Details of the conditioning cycle are described in a previous communication.[12] The magnitude of the Fourier transforms of the k^2-weighted EXAFS spectra for the In and Sb edges are shown in Figs. 3(a) and 3(b). At 1.41 V, the In- and Sb-edge spectra are similar, owing to the fact that In and Sb differ by only two atomic numbers and have the same neighboring atoms within the InSb structure. The spectra are also consistent with EXAFS from an InSb standard.[12] The most significant contribution to the EXAFS spectrum clearly occurs at the positions of the In-Sb and Sb-In nearest-neighbor (nn) paths, (*I*) and (*V*), respectively. Only slight changes are discernible while discharging the cell to 0.72 V. Between 0.72 and 0.66 V, In is observed to be replaced by Li, as evidenced most clearly by the growing contribution of the Sb-Li path (*IV*). The most drastic changes occur between 0.66 V and 0.53 V, the potential range in which In is extracted from the InSb lattice and replaced by Li. The In-Sb path (*I*) of the In-edge data is now clearly dominated by the two closest In metal paths, summarily represented by (*III*) in Fig. 3(a). This becomes particularly apparent if the much larger DW factor of the metal path is taken into account. Accordingly, the Sb-In path (*V*) of the Sb-edge data is now dominated by the Sb-Li path (*IV*). As will be discussed below for the higher quality data of cell B, starting at around 0.55 V, the extruded In metal is lithiated as well. The data from cell A are too noisy to show unambiguously the contribution of the In-Li path.

The quality of the EXAFS data was improved during the second experiment, the charging and discharging of cell B, primarily due to increased stability of the beam. Among other improvements, this allows for including the second-shell data of the Sb-edge EXAFS, key to demonstrating that the Sb remains in a fcc sublattice. In related *ex situ* experiments, at low temperature, where the lattice vibrations are

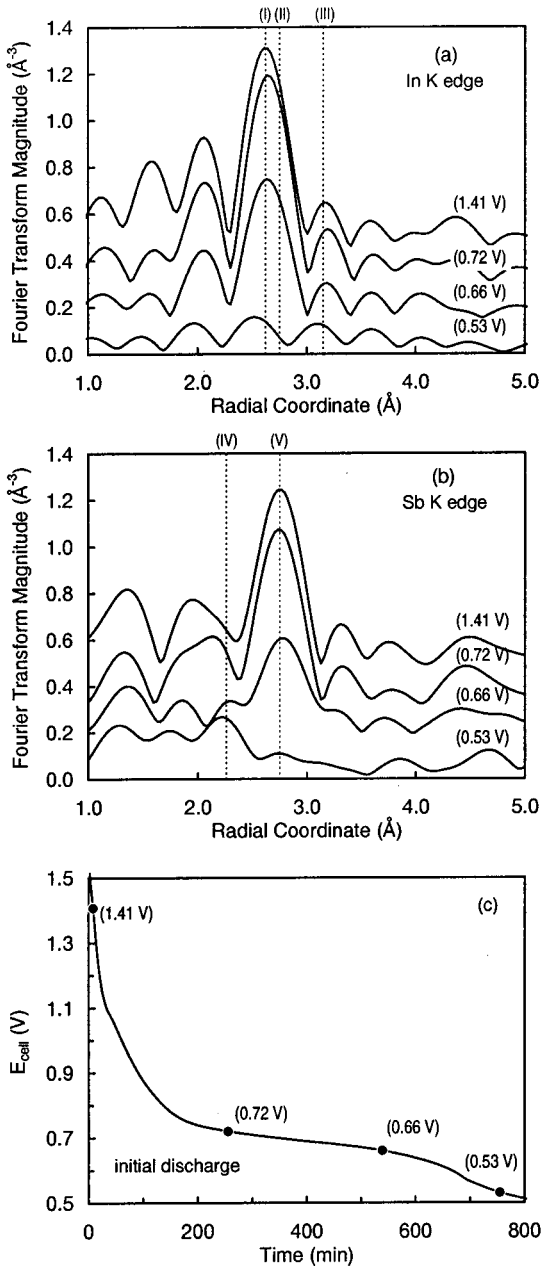

FIG. 3. Freshly prepared Li/InSb coin cell during the initial conditioning cycle (cell A). EXAFS data are shifted for clarity. (a) Fourier transform of the k^2-weighted In-edge EXAFS spectra at selected cell potentials. First-shell scattering paths are indicated by dotted lines: (*I*) In-Sb nearest neighbor (nn) path in InSb, (*II*) In-In nn path in Li_xIn, and (*III*) In-In nn path in indium metal. (b) Fourier transform of the k^2-weighted Sb-edge EXAFS spectra at selected cell potentials. First-shell scattering paths are indicated by dotted lines: (*IV*) Sb-Li nn path in Li_3Sb and (*V*) Sb-In nn path in InSb. For information on the EXAFS data windows, see the caption of Fig. 4. (c) Galvanostatic potential vs. time curve (current density 0.3 mA/cm^2).

significantly reduced, the Sb-Sb shell can be fit much more accurately.[19] These measurements further confirm the stability of the fcc Sb sublattice under similar cycling conditions. The galvanostatic potential vs time curve for charging cell B is shown in Fig. 4(c), and the magnitude of the Fourier transform of representative k^2-weighted EXAFS spectra for the In as well as Sb edges are shown in Figs. 4(a) and 4(b). Finally, in Fig. 4(d) the raw $k^2\chi(k)$ data are displayed along with the fit for two representative Sb-edge EXAFS spectra. This demonstrates the quality of the fit of the data to the selected theoretical paths.

The spectra at 0.63 V represent the state of coin cell B at the beginning of the charge cycle. The Sb-edge data shown in Fig. 4(b) are clearly dominated by the Sb-Li nn path (*IV*). A quantitative analysis of the path contribution [i.e. the contribution of N_i in Eq. (3)] shows that Sb has about 90% Li nearest neighbors, while less than 10% of the In nearest neighbors remain. Accordingly, the In-edge EXAFS show only a weak indication of Sb neighbors [less than 10%, path (*I*)], while the dominant contribution is the nearest-neighbor In-In path from Li_xIn (*II*). Obviously, indium had not only been cycled out of InSb, but metallic In had also been lithiated in a parallel reaction during the off-line conditioning reaction.

Upon charging the cell from 0.63 to 0.79 V, no significant changes are observed in the Sb-edge EXAFS. Antimony is still predominantly coordinated by Li, and little or no Li has been extracted from the Sb fcc framework. The lithiated In, on the other hand, undergoes a phase transformation. The Li_xIn, In-In path (*II*) that dominated at 0.63 V is all but gone, and strong contributions from the In-In metal nn paths (*III*) are observed. About 80% of the In now prevails as In metal, while only 10% of the In is lithiated, with the remaining In still localized in the Sb framework. The next phase transformation occurs between 0.89 and 0.94 V and involves both In and Sb. The plateau in the potential vs time curve in Fig. 4(c) indicates a two-phase reaction,[7] but only analysis of the EXAFS spectra elucidates the microscopic mechanism of this phase transition. The Sb-edge EXAFS first-shell data show a clear shift from the Sb-Li nn path (*IV*) to the Sb-In nn path (*V*). Obviously, Li is now extracted from the Sb fcc framework, and In is reinserted into its original lattice sites (c), from Fig. 1. Overall, the EXAFS spectrum of the lithiated InSb electrode begins to resemble the InSb standard upon reaching the charged state. The In-edge EXAFS is consistent with this phase transformation, showing the growing In-Sb nn path (*I*) and a decreasing contribution from the In-In metal nn path (*III*). This phase transformation back to a defect InSb structure is complete when the cell is fully charged; i.e., virtually all Li has been removed. At 1.1 V, the Sb-In nn path (*V*) dominates the Sb EXAFS, while the In-Sb nn path (*I*) dominates the In-edge EXAFS. An analysis of the path contribution shows that in the fully charged state, about 60% of the In prevails as InSb, while 40% remains outside the electrode as In metal (most likely localized at the grain boundaries of the ball-milled InSb). The Sb-edge data confirm this picture, with 60% of the Sb nn tetrahedral sites occupied by In. In addition, further structural information about the fully charged Li/InSb electrode can be extracted from the Sb-edge spectra. Surprisingly. the contribution from the Sb-Li nn path (*IV*) is much weaker than would be expected for a lattice in which the remaining 40% of the Sb neighbor sites were coordinated by Li. In fact, the Sb-Li path contributes less than 20% to the Sb-edge EXAFS (the best fit

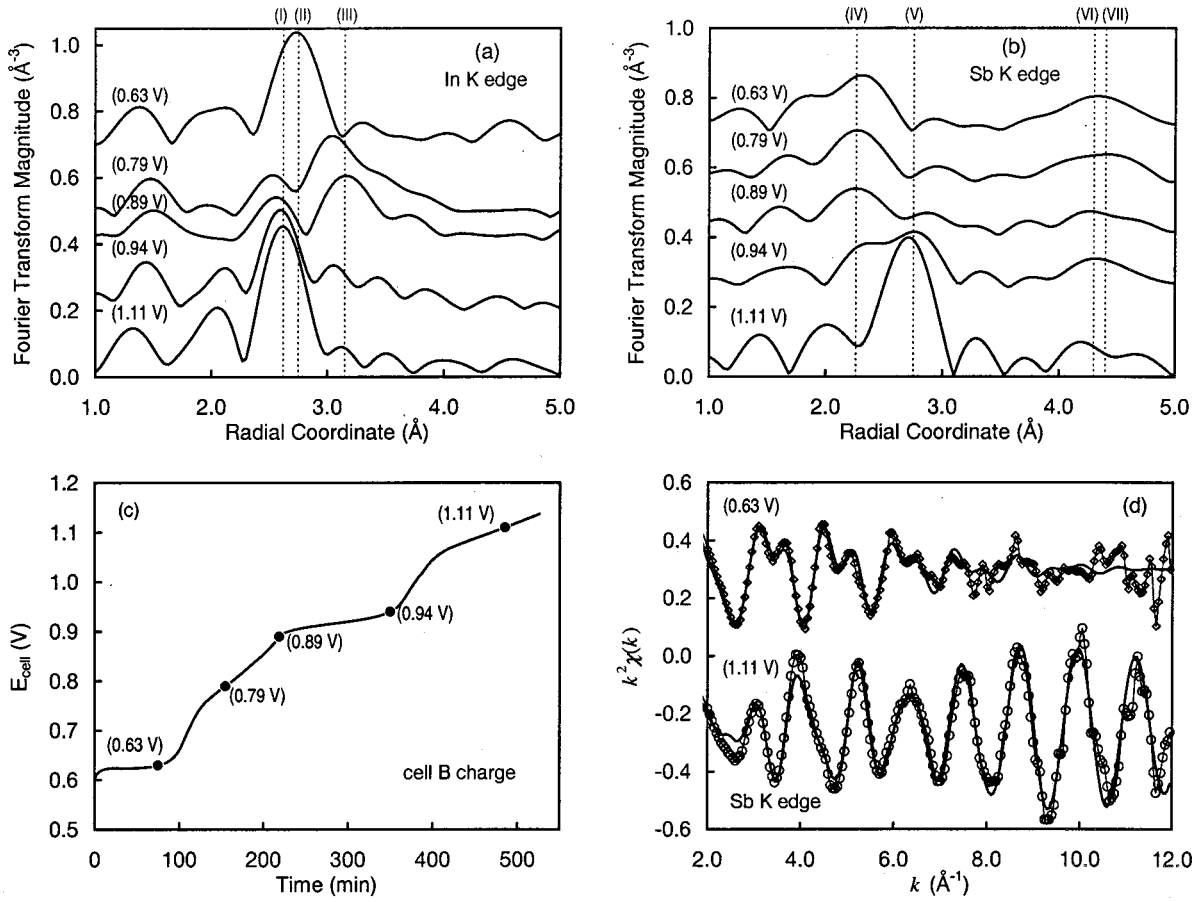

FIG. 4. Charging of a preconditioned Li/InSb coin cell (cell B). (a) Fourier transform of the k^2-weighted In-edge EXAFS spectra at selected cell voltages. Scattering paths are indicated by dotted lines as described in the caption for Fig. 3. (b) Fourier transform of the k^2-weighted Sb-edge EXAFS spectra at selected cell voltages. Scattering paths are indicated by dotted lines: (*IV*) Sb-Li nn path in Li_3Sb, (*V*) Sb-In nn path in InSb, (*VI*) Sb-Sb next-nearest-neighbor (nnn) path in InSb, and (*VII*) Sb-Sb nnn path in Li_3Sb. (c) Galvanostatic potential vs time curve for charging at a constant current density (0.4 mA/cm^2). (d) k^2-weighted raw Sb-edge EXAFS data (open symbols and thin lines) together with the fit of the sum of the paths (thick solid line). The EXAFS data windows are set as follows: 2.8 Å$^{-1}\leqslant k\leqslant$11.2 Å^{-1} and 1.8 Å$\leqslant R\leqslant$3.8 Å for In-edge data, and 2.0 Å$^{-1}\leqslant k\leqslant$10.5 Å^{-1}, and 1.9 Å$\leqslant R\leqslant$5.0 Å for Sb-edge data.

is less than 5%), leading to the conclusion that at least 20% of the In sites in InSb now prevail as Schottky vacancies, suggesting a defect zinc-blende structure with the composition $In_{0.6}Li_{0.05}\square_{0.35}Sb$, where $\square$ refers to a vacancy. The large uncertainties are due to the very small contribution of the Sb-Li paths to the EXAFS.

The phase transformations that have been described for the charge cycle are essentially reversed when the cell is discharged (see Fig. 5). However, as will be discussed in more detail in Sec. V, the voltages at which those transformations occur are shifted. In addition, the cell has been discharged to 0.10 V in order to obtain more information on the lithiation of the In metal phase, which starts below 0.60 V. The In- and Sb-edge spectra obtained at 0.93 V during discharging are essentially identical to the spectra discussed for the fully charged cell in the previous paragraph; Sb has about 60% In nearest neighbors and less than 20% Li neighbors, and the remaining lattice positions apparently remain vacant, while 40% of the In prevails as metal at the grain boundaries of the InSb electrode. From 0.93 to 0.69 V, Li is inserted into the Sb fcc sublattice without any measurable extrusion of In. Upon discharging from 0.69 V to 0.57 V, the Sb-Li nn path (*IV*) becomes prominent for the Sb-edge spectra, and In metal [path (*III*)] starts to dominate the In-edge spectra; i.e., indium is extruded from the InSb electrode and replaced by Li. While the lithiation of the Sb fcc host lattice is completed around 0.60 V and no more significant changes are observed in the Sb-edge spectra, the In-edge spectra give valuable information about the transformation of the extruded In metal phase. Between 0.57 and 0.10 V, the In metal phase is fully lithiated, forming various Li_xIn phases. The formation of Li_xIn is visible in the In-edge EXAFS spectra as the disappearance of the In-In metal nn contribution (*III*) and the dominance of the In-In nn path (*II*) in Li_xIn. Three lithiated indium phases have In-In distances consistent with the measured In-In distances: LiIn (2.94 Å), Li_3In_2 (2.97 Å), and Li_2In (2.92 Å).

Additional information has been obtained from analyzing the near-edge portion of the XAFS spectra (XANES).[13,15] In particular, the edge energy, as measured by the energy at 50% of the normalized edge step, has been employed as an indication of the oxidation state of In and Sb. This edge shift

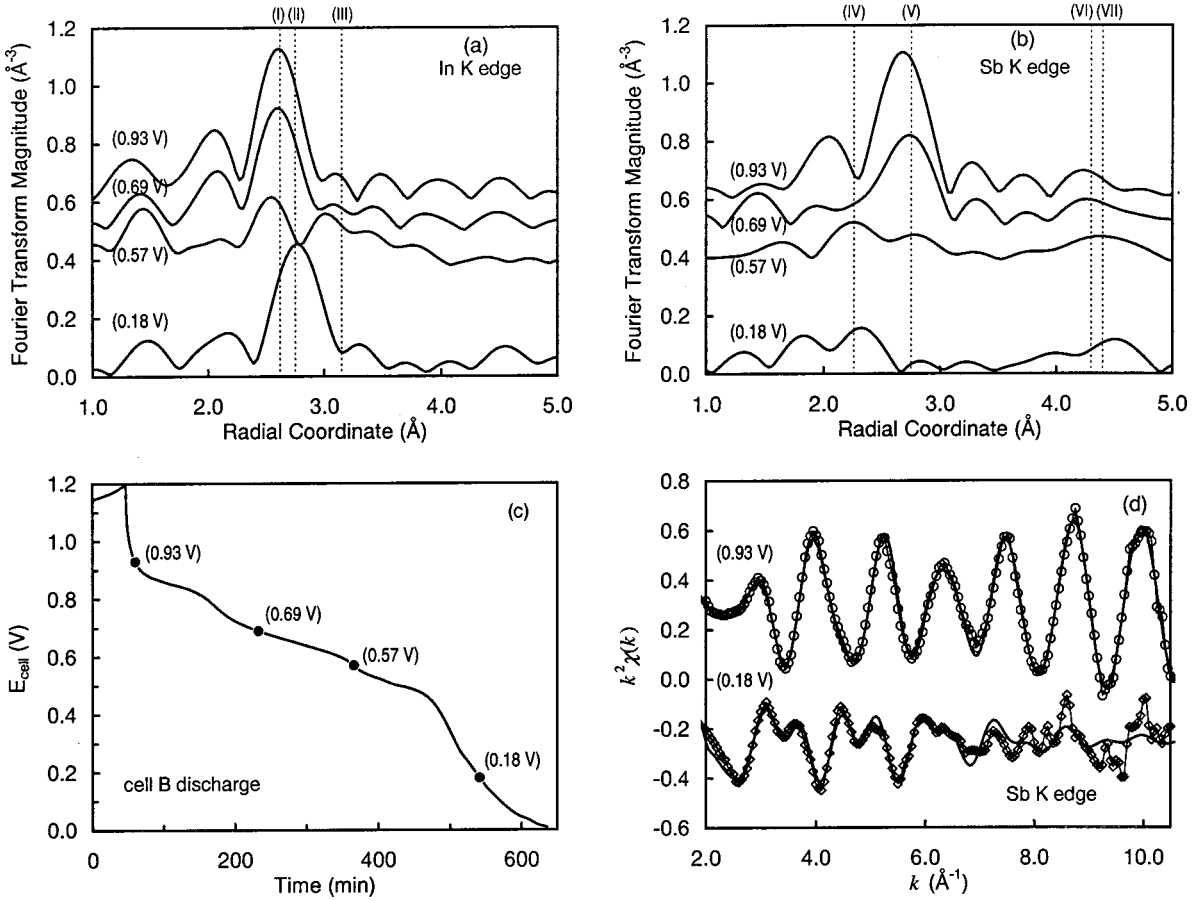

FIG. 5. Discharging of a preconditioned Li/InSb coin cell (cell B). (a) Fourier transform of the k^2-weighted In-edge EXAFS spectra at selected cell voltages. Individual scattering paths are marked with dotted lines and explained in Fig. 4. (b) Fourier transform of the k^2-weighted Sb-edge EXAFS spectra at selected cell voltages. (c) Galvanostatic potential vs time curve upon discharging at a constant current density of 0.5 mA/cm^2. (d) k^2-weighted raw Sb-edge EXAFS data (open symbols and thin lines) together with the fit of the sum of the paths (thick, solid line). For information about the EXAFS data windows, see the caption of Fig. 4.

is calibrated by measuring the edge position of standard components in different oxidation states. For example, for the In edge the standards In(0) in indium metal, In(I) in InCl, and In(III) in In_2O_3 have been measured. From these calibration experiments, we infer that an edge shift of about 2 eV corresponds to a change in formal oxidation state by one. Comparing the edge position for indium metal with LiIn and InSb shows that the the edge positions are 0.7 $\pm$0.1 eV and 1.2$\pm$0.1 eV higher than indium metal, respectively. Both of these observed edge shifts are smaller than a change in the oxidation state by one. The edge shifts observed for In and Sb during charging and discharging a lithiated InSb coin cell electrode are shown in Figs. 6(b) and 7(b), and will be discussed in more detail in Sec. V.

V. DISCUSSION

This section offers a detailed analysis of the EXAFS and XANES data with emphasis on changes in composition, bond length, and oxidation state of the InSb electrode in different states of lithiation. While only representative EXAFS spectra have been presented in the previous section, the analysis of the phase transformations presented here will include all data to highlight the continuous nature of the phase transitions.

Charge cycle

The predominant electrochemical reaction during charging a Li/InSb coin cell is the extraction of Li from the lithiated InSb electrode. The XAFS data presented here allow one to identify the microscopic mechanism of several separate phase transformations driven by this delithiation. The fractions of the different phases (lithiated InSb, In metal, and Li_xIn) as represented by the contribution of the different scattering paths, N_i, from Eq. (3), are shown in Fig. 6(c). While charging the cell, the first phase transformation occurs between 0.6 and 0.7 V and can be assigned, predominantly, to the delithiation of Li_xIn. The Li_xIn content represented by the nearest-neighbor In-In path (filled squares) falls from about 70% to zero, while the In metal phase fraction (filled circles) rises from about 20% to its maximum value of 90%. The nature of this phase transformation is corroborated by the XANES data shown in Fig. 6(b). The indium edge energy decreases by about 0.8 eV, corresponding to approximately

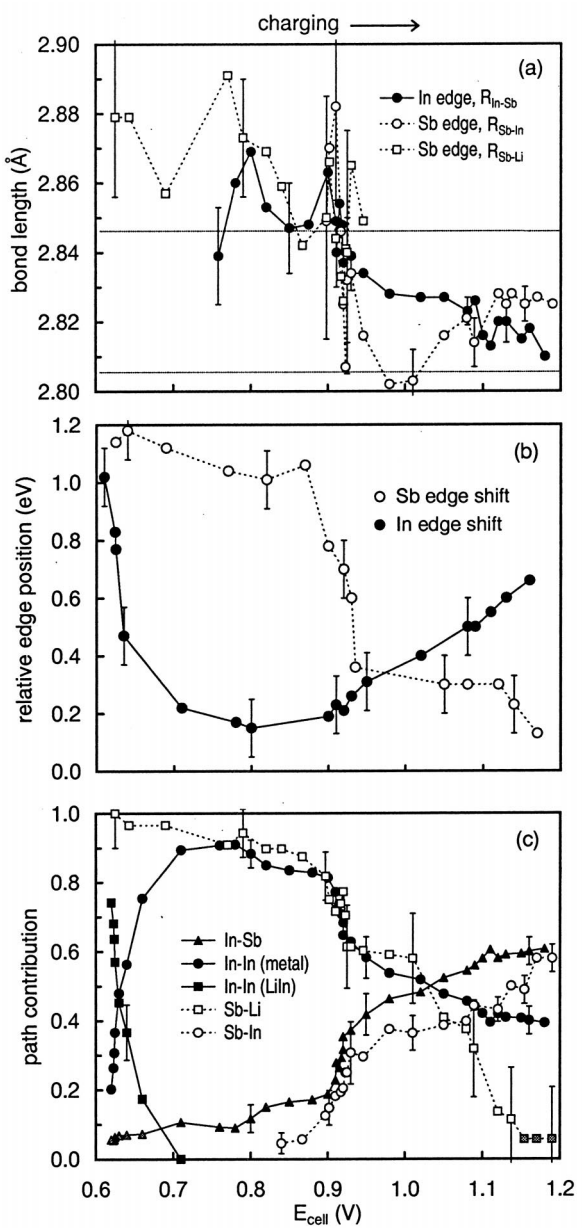

FIG. 6. Charging of a preconditioned Li/InSb coin cell (cell B). Changes in composition, edge position, and lattice spacing are shown as a function of cell voltage, i.e., degree of lithiation. (a) Bond length of the Sb-In nearest-neighbor pairs as obtained from the In-edge, In-Sb path and the Sb-edge, Sb-In, and Sb-Li paths. The lower dotted line represents the crystallographic In-Sb distance in pure InSb, while the upper dotted line represents the crystallographic Sb-Li distance in pure Li_3Sb. (b) Relative shift of the edge position for Sb- and In-edge XANES. (c) Phase fractions based on the path contribution to the EXAFS spectra for the InSb phase (Sb-In and In-Sb nn path), metallic In (In-In nn path), Li_xIn (In-In nn path) and lithiated InSb as represented by Li_3Sb (Sb-Li nn path). The shaded squares for the Sb-Li path and the shaded triangles for the In-Sb path are not the result of a fit minimization.

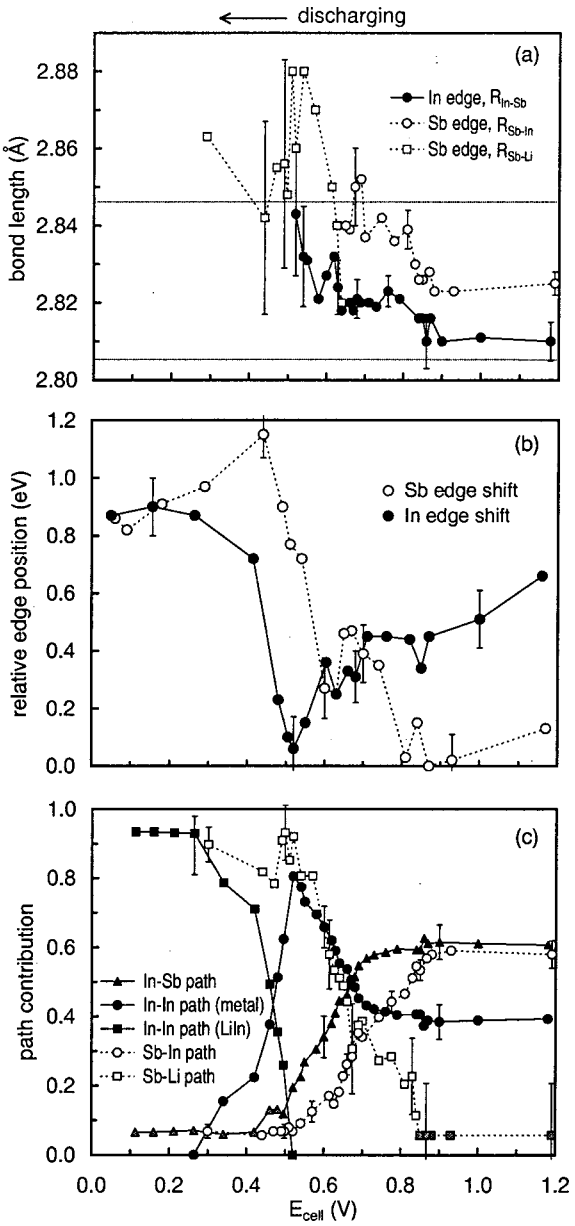

FIG. 7. Discharging of a preconditioned InSb/Li coin cell (cell B). (a) Bond length of the Sb-In nearest-neighbor pairs as obtained from the In-edge, In-Sb path and the Sb-edge, Sb-In and Sb-Li paths. (b) Relative shift of the edge position for Sb- and In-edge XANES. (c) Phase fractions based on the path contribution to the EXAFS spectra for InSb phase (Sb-In and In-Sb nn paths), metallic In (In-In nn path), Li_xIn (In-In path), and lithiated InSb represented by Li_3Sb (Sb-Li nn path). The shaded squares for the Sb-Li path and the shaded triangles for the In-Sb path are not the result of a fit minimization.

one-half of an oxidation state. This is consistent with the formation of indium metal from LiIn.

While the In-edge XAFS reflects those changes, the Sb-edge XAFS spectra are virtually unaffected by the reaction, supporting the notion that In metal and Li_xIn are separate phases precipitated at the grain boundaries of the lithiated InSb electrode. This scenario is consistent with the following observations: (i) The amount of lithiated InSb is represented by the Sb-Li path (open squares) obtained from FEFF calculations for Li_3Sb but should be described more accurately as $Li_{x+y}In_{1-y}Sb$ since as much as 10% of the In remains within the InSb framework. The Sb-Li contribution remains at

around 90% in the voltage range from 0.6 V to 0.9 V, unaffected by the delithiation of Li_xIn. In the same range, the number of In neighbors around Sb (open circles) remains less than 10%. (ii) The oxidation state of Sb [open circles in Fig. 6(b)] does not change appreciably between 0.6 and 0.9 V.

The second phase transformation, which now affects the entire Li/InSb electrode occurs in the narrow voltage range from 0.90 to 1.05 V. Here the In metal content rapidly falls from 90% to 50%, while the In content in the Sb fcc framework increases from less than 10% to 50%, as indicated by both the Sb-In nn path (open circles) and the In-Sb nn path (filled triangles) in Fig. 6(c). Concurrently, the Sb-Li nn contribution (open squares) decreases from 90% to 50%. Clearly, Li is extracted from the Sb fcc framework and replaced by In. In the same voltage range, the formal oxidation state of Sb is reduced by about one-half. While this is not a large change in oxidation state, it can be explained consistently in terms of electron affinity, the energy gained by an atom in a crystal when an electron is added.[20,21] The electron affinities of Sb, In, and Li are 1.07, 0.30, and 0.62 eV, respectively.[20] Therefore, it is expected that Sb will be reduced if most of the Li neighbors are replaced by In, which possesses only half the electron affinity of Li. The fact that this phase transformation takes place in the lithiated InSb electrode is supported by the changes in the In-Sb bond length; below 0.90 V, Sb is mostly surrounded by Li, and the distance between an Sb lattice point and its nearest neighbor (the site occupied by indium in InSb, but mostly Li in the case of the almost completely lithiated $Li_{x+y}In_{1-y}Sb$ electrode) is best described by the Li-Sb distance in Li_3Sb taken from crystallographic data,[22] and indicated by the upper dotted line in Fig. 6(a).

Above 0.90 V, Sb is mostly surrounded by In, and the nn distance decreases, closer to the crystallographic In-Sb spacing found for InSb (2.805 Å),[22] as indicated by the lower dotted line. As is apparent from Fig. 6(a), this expectation is indeed supported by the change in bond length provided by the EXAFS data. The fact that Li extraction and In reinsertion alters the In-Sb bond length quasicontinuously indicates that the phase transformation takes place rather uniformly within the Sb framework, as suggested Sec. I. If distinct regions of Li_3Sb and InSb prevailed and only their ratio changed, as in a reaction propagating inward from a particle's surface, the In-Sb distance would remain constant as Li_3Sb and In would react to form InSb and Li.[12] This scenario is not supported by our experimental evidence, nor is it consistent with the recent interpretation of the electrochemical reaction of InSb with Li as given by Hewitt *et al.*[23]

The final reaction associated with charging the cell takes place between 1.05 and 1.15 V. In this region, Li extraction and In reinsertion are completed, and, in the fully charged state, about 60% of the In has been reinserted into the Sb fcc framework, as evidenced by both the Sb-In nn path [open circles in Fig. 6(a)] and the In-Sb nn path (filled triangles). The fact that about 40% of the In remains outside of the InSb electrode as indium metal explains the partial loss in battery capacity that is observed for the Li/InSb cell after the conditioning cycle.[7] In parallel to the completion of the In reinsertion, Li is extracted, relatively much more rapidly, from the interstitial sites of InSb [(b) and (d) in Fig. 1]. This is indicated by the fact that the contribution of the Sb-Li nn path [open squares in Fig. 6(a)] decreases more rapidly (from 50% at 1.05 V to less than 5% at 1.15 V) than the contribution from the Sb-In path. This reaction yields an In-deficient zinc-blende structure, $Li_xIn_{1-y}Sb$ at the top of charge. In the fully charged state, Sb has 60% In neighbors and less than 5% Li neighbors, with the result that more than 35% of the In sites in InSb remain vacant. Indium has 60% Sb neighbors, i.e., 60% of the In prevails in InSb, and about 40% of the In remains outside the InSb electrode as In metal. As mentioned earlier, because of the very small amplitude of the Sb-Li path, as much as 20% could be included in the fit, while only doubling the *R*-factor, a measure of the goodness of the fit.

From 0.9 to 1.2 V the In edge position shifts upward by 0.4 eV. This is consistent with the formation of InSb, which has an edge energy 1.2 eV higher than In metal. Since about 40% of the indium remains metallic, the edge energy doesn't shift entirely to the InSb edge energy.

Discharge cycle

Phase fractions, edge shifts, and In-Sb bond lengths as obtained from Sb- and In-edge XAFS for the discharge of cell B, are shown in Fig. 7. Note that the figure needs to be read from right to left to account for the switch from charging to discharging. The predominant electrochemical reaction for discharge is the insertion of Li into the negative electrode. The phase distribution of the fully charged cell was described in the previous paragraph. Upon discharging, the aforementioned phase transitions are essentially reversed. However, these reactions occur at a lower cell potential compared to the charge cycle. This hysteresis is due to nonequilibrium polarization effects of the electrode. Such overpotential effects are characteristic of electrode processes and are exacerbated in this case by the presence of multiple phases. For example, Li insertion into interstitial sites does not occur until a potential of about 0.90 V is reached. It is only then that the Sb-Li path [open squares in Fig. 7(c)] starts to rise from zero, and the lattice expands slightly as indicated by the increase in R_{InSb} and R_{SbIn} in Fig. 7(a). Between 0.90 and 0.70 V, Li insertion occurs without any significant In extrusion. Indium metal starts to be extruded from the Sb fcc framework at around 0.70 V and the In metal contribution reaches its peak of about 85% at 0.52 V as indicated by the maximum contribution of the In-In path (filled circles). Concurrent with the extrusion of indium from the Sb fcc framework, Li is inserted as shown by the increase in the Sb-Li path contribution (open squares).

At around 0.70 V, the shift of the Sb edge shown in Fig. 7(b) indicates a partial oxidation of the Sb by about one-half of a formal oxidation state. This is consistent with the fact that the electron donor indium is replaced by Li, which has a greater electron affinity. Lithium insertion and In extraction are completed at around 0.51 V. Despite these drastic changes in composition, the bond length between Sb and the

TABLE II. Cell potential ranges and primary reactions in the Li/InSb electrochemical cell.

Cell	Potential (V)	Primary reaction
A	1.4→0.7	$x\mathrm{Li}+\mathrm{InSb}\rightarrow \mathrm{Li}_x\mathrm{InSb}$
(discharge)	0.7→0.5	$z\mathrm{Li}+\mathrm{Li}_x\mathrm{InSb}\rightarrow \mathrm{Li}_{x+z}\mathrm{In}_{1-y}\mathrm{Sb}+y\mathrm{In}$
B	0.6→0.7	$\mathrm{Li}_x\mathrm{In}\rightarrow x\mathrm{Li}+\mathrm{In}$
(charge)	0.7→0.95	$y\mathrm{In}+\mathrm{Li}_3\mathrm{Sb}\rightarrow x\mathrm{Li}+\mathrm{Li}_{3-x}\mathrm{In}_y\mathrm{Sb}$
	0.95→1.2	$(0.6-y)\mathrm{In}+\mathrm{Li}_x\mathrm{In}_y\mathrm{Sb}\rightarrow x\mathrm{Li}+\mathrm{In}_{0.6}\mathrm{Sb}$
B	1.2→0.9	$x\mathrm{Li}+\mathrm{In}_{0.6}\mathrm{Sb}\rightarrow \mathrm{Li}_x\mathrm{In}_{0.6}\mathrm{Sb}$
(discharge)	0.9→0.5	$(3-x)\mathrm{Li}+\mathrm{Li}_x\mathrm{In}_{0.6}\mathrm{Sb}\rightarrow 0.6\mathrm{In}+\mathrm{Li}_3\mathrm{Sb}$
	0.5→0.1	$x\mathrm{Li}+\mathrm{In}\rightarrow \mathrm{Li}_x\mathrm{In}$

original In site in InSb, now mostly occupied by Li, has expanded by only $2.7\pm0.7\%$. This implies an overall volume expansion of about 8%, and highlights the capability of the Sb fcc host lattice to accommodate large amounts of the alkali metal. In this respect, InSb compares favorably to graphite as a host for Li, and provides one important prerequisite for replacing graphite intercalation electrodes by intermetallic compound insertion electrodes.

Below 0.51 V, the In metal phase begins to be lithiated. This is evident from the decrease of the In-In metal path (filled circles) and the increase of the In-In ($\mathrm{Li}_x\mathrm{In}$) path (filled squares). This phase transformation is accompanied by oxidation of the In, as indicated by the edge shift shown in Fig. 7(b) (filled circles). Again, the oxidation is due to the addition of Li, a neighbor with a greater electron affinity than In. The magnitude of this change is comparable to the increase in edge position measured between indium metal and LiIn. This reaction is essentially completed at about 0.30 V, where less than 10% of the In is present as InSb, while both Sb (still forming a stable fcc lattice but now in a superlattice with a composition close to $\mathrm{Li}_3\mathrm{Sb}$) and In (now forming almost completely lithiated $\mathrm{Li}_x\mathrm{In}$) have about 90% Li neighbors. At these low voltages, the contributions from the Sb-In and In-Sb paths are too weak to yield reliable bond lengths. However, the Sb-Li bond length can be extracted from Sb-edge EXAFS [open squares in Fig. 7(a)], and is consistent with a bond length close to the 2.846 Å expected for $\mathrm{Li}_3\mathrm{Sb}$. It has to be emphasized again that, although InSb has been almost completely converted to $\mathrm{Li}_3\mathrm{Sb}$, the original Sb fcc framework remains intact without rearranging the lattice points (see Fig. 1), and the Sb-Li spacing is still close to the original Sb-In spacing for unlithiated InSb. The EXAFS data clearly support the notion that InSb transforms smoothly and continuously into $\mathrm{Li}_3\mathrm{Sb}$ upon lithiation. Theoretically, $\mathrm{Li}_2\mathrm{Sb}$ could form as an additional phase during the lithiation of InSb. However, $\mathrm{Li}_2\mathrm{Sb}$ is not commensurate with the InSb superlattice shown in Fig. 1. Attempts to fit $\mathrm{Li}_2\mathrm{Sb}$ paths to the data have given no indication of the presence of $\mathrm{Li}_2\mathrm{Sb}$ in lithiated InSb at any cell potential. Table II summerizes the primary reactions that occur as a function of the cell potential over the charge and discharge cycles.

A closer evaluation of the data presented in Figs. 6 and 7 reveals a number of troubling inconsistencies. First of all, in Figs. 6(a) and 7(a), R_{InSb} and R_{SbIn} should be equal within the stated error. The more or less constant offset in Fig. 7(a) can be explained as a limitation in the theoretical calculation that has not been properly accounted for. However, in Fig. 6(a), the bond lengths change in opposite directions as a function of potential. The second inconsistency is in the path contributions, N_{InSb} and N_{SbIn}. These should also be equal at all times. In Fig. 6(c), the offset could again be explained as merely a calibration error, exacerbated by the multiple phases present. In Fig. 7(c), the constant shift is along the x axis (cell potential) rather than the y axis. This is a much more difficult difference to explain, likely revealing some limitation in the model. We investigated an alternative approach, simultaneously fitting multiple sets of data, constraining certain fit parameters. By constraining $R_{InSb}=R_{SbIn}$ and $N_{InSb}=N_{SbIn}$, this technique resulted in unacceptably poor fits.

Stability of the Sb host lattice

An important constant factor throughout the entire range of electrochemically induced phase transformations is the stability of the Sb fcc host lattice. We have attempted to fit the EXAFS spectra with the inclusion of a metallic Sb-Sb path. At no cell potential is it possible to obtain a self-consistent description of the EXAFS spectra if an Sb-Sb metal path is included. This finding can be visualized by comparing the raw EXAFS data to EXAFS spectra from standards as shown in Fig. 8. Here the k^2-weighted EXAFS spectra for In metal (a), InSb powder (b), and Sb metal (c) are shown as solid lines. As expected, the In metal EXAFS is close to the In-edge EXAFS from coin cell B charged to 0.8 V [dotted line in Fig. 8(a)]. At this state of charge, about 90% of the indium prevails as metal.

Similarly, the In-edge EXAFS from an InSb standard is reasonably consistent with both the Sb-edge EXAFS [dotted line in Fig. 8(b)] and the In-edge EXAFS [dashed line in Fig. 8(b)] obtained from a fully charged Li/InSb coin cell (1.2 V). At this state of charge, the highest InSb content of 60% is reached. The difference in amplitude between the standard and the sample is explained by the smaller contribution of the In-Sb path in the case of the charged coin cell. The apparent similarity of the In- and Sb-edge EXAFS at this particular cell potential is due to the fact that In and Sb differ by only two atomic numbers and have the same neighbors around each other, resulting in a similar backscattering function $f(k)$ [see Eq. (3)].[12] Finally, in Fig. 8(c), the EXAFS from Sb metal is shown (solid line). This EXAFS spectrum is different than the Sb-edge spectrum at 1.2 V [see Fig. 8(b)]

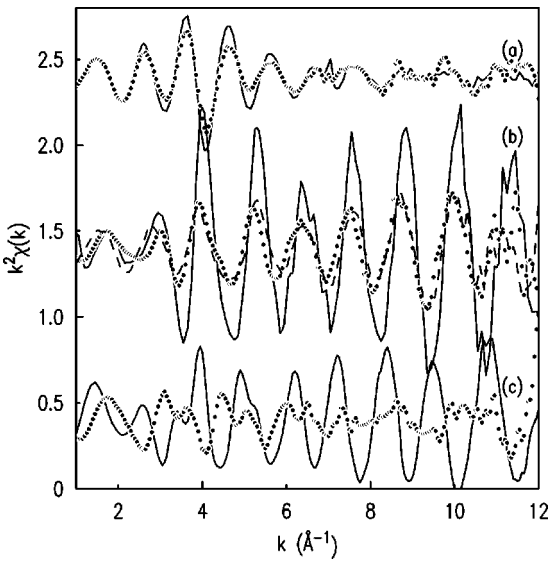

FIG. 8. k^2-weighted raw EXAFS data for (a) In metal standard (solid line) and Li/InSb electrode of cell B at 0.8 V during charging (dotted line, In-edge EXAFS), (b) InSb standard (solid line, In-edge EXAFS) and Li/InSb electrode of cell B at 1.2 V during charging (dotted line: Sb-edge EXAFS, dashed line: In-edge EXAFS), and (c) Sb metal standard (solid line) and Li/InSb electrode of cell B at 0.1 V during discharging (dotted line: Sb-edge EXAFS).

and also from the spectrum obtained for the fully discharged cell at 0.1 V shown as a dotted line in Fig. 8(c). Apparently, no indication of Sb metal beyond the EXAFS detection limit (approx. imately 5%) is found for Li/InSb over the entire potential range including the fully charged and discharged states. As opposed to In, which occupies between 10% and 60% of the zinc-blende lattice positions in InSb, the Sb occupancy remains close to 100% at all potentials.

VI. CONCLUSIONS

We have demonstrated that x-ray absorption spectroscopy provides detailed microstructural information about electrochemically induced phase transformations that occur in InSb upon lithiation and delithiation. Discharge of a Li/InSb coin cell results in Li insertion into the electrode in three separate steps occurring at decreasing values for the cell potential: (i) Li is inserted in lattice sites interstitial to InSb, (ii) Li replaces In that is extruded from its InSb lattice sites, and finally (iii) Li is reacted with the extruded In metal. These phase transitions are essentially reversed upon changing the direction of the current, i.e., upon charging the cell. The potentials at which the phase transitions occur are shifted relative to the discharge cycle due to polarization effects at the electrode. Our EXAFS data show that in the fully charged state, about 40% of the In remains permanently outside the Sb fcc framework, and more than 20% of the In sites in InSb remain unoccupied.

Despite the drastic changes in coordination experienced by Sb, from $<20\%$ Li, $>20\%$ vacancies, and 60% indium in the charged state to almost 100% Li in the discharged state, the Sb host lattice remains remarkably stable at all cell potentials. This stability of the host lattice together with the compatibility of the phases that transform continuously into each other—InSb, $Li_{x+y}In_{1-y}Sb$, and almost fully lithiated Li_3Sb—is one reason why this type of intermetallic electrode is such an intriguing host for Li. An additional important reason for the ease with which these phase transformations occur is the absence of significant changes in oxidation state and, therefore, the absence of charge transfer. The formal oxidation state of Sb and In, as probed by XANES, changes by no more than one-half over the entire potential range, indicating that electrons are essentially shared; replacing In by Li in InSb (or vice versa) does not change the electronic structure of the Li/InSb system in a significant way.

Intermetallic compound electrodes such as InSb are different from graphite electrodes with respect to the absence of a layered structure that is able to intercalate alkali metal atoms. In the case of InSb, alkali-metal atoms are incorporated into a slightly expanded but stable Sb fcc host lattice after the second component, indium, has been extruded from the lattice. It should be noted that InSb, which crystallizes in the zinc-blende structure, has a relatively open network, providing diffusion paths for the Li to be inserted into the structure; the volume occupied by hard spheres in the zinc-blende structure is only 34%, while the value is 74% for closest packed cubic structures.

ACKNOWLEDGMENTS

Support for this work from the U.S. Department of Energy, Office of Basic Energy Sciences, Division of Chemical Sciences, under Contract No. W-31-109-Eng-38 is gratefully acknowledged. The Advanced Photon Source is supported by the U.S. Department of Energy, Basic Energy Sciences, Office of Science (DOE-BES-SC), under Contract No. W-31-109-Eng-38. MRCAT is funded by its member institutions and DOE-BES-SC under Contract Nos. DE-FG02-94ER45525 and DE-FG02-96ER45589.

*Electronic address: kropf@cmt.anl.gov

[1] H. Zabel and S.A. Solin, *Graphite Intercalation Compounds* (Springer-Verlag, Berlin, 1990).

[2] For a review on intercalation compounds, see H. Selig and L.E. Ebert, Adv. Inorg. Chem. Radiochem. **23**, 281 (1980).

[3] R. Yazami and P. Touzain, J. Power Sources **9**, 365 (1983).

[4] R.A. Huggins, J. Power Sources **81-82**, 13 (1999).

[5] K.D. Kepler, J.T. Vaughey, and M.M. Thackeray, Electrochem. Solid-State Lett. **2**, 307 (1999).

[6] J. Yang, Y. Takeda, N. Imanishi, and O. Yamamoto, J. Electrochem. Soc. **146**, 4009 (1999).

[7] C.S. Johnson, J.T. Vaughey, M.M. Thackeray, T. Sarakonsri, S.A. Hackney, L. Fransson, K. Edstrøm, and J.O. Thomas, Electrochem. Commun. **2**, 595 (2000).

[8] J.T. Vaughey, J.O. O'Hara, and M.M. Thackeray, Electrochem. Solid-State Lett. **3**, 13 (2000).

[9] D. Larcher, L.Y. Beaulieu, D.D. MacNeil, and J.R. Dahn, J. Electrochem. Soc. **147**, 1658 (2000).

[10] M.M. Thackeray, J.T. Vaughey, C.S. Johnson, A.J. Kropf, H. Tostmann, T. Sarakonsri, and S.A. Hackney, Electrochem. Soc. Proc. **2000-36**, 92 (2000).

[11] J.T. Vaughey, C.S. Johnson, A.J. Kropf, R. Benedek, M.M. Thackeray, H. Tostmann, T. Sarakonsri, S. Hackney, L. Fransson, K. Edstrøm, and J.O. Thomas, J. Power Sources **97-98**, 194 (2001).

[12] A.J. Kropf, H. Tostmann, C.S. Johnson, J.T. Vaughey, and M.M. Thackeray, Electrochem. Commun. **3**, 244 (2001).

[13] J.J. Rehr and R.C. Albers, Rev. Mod. Phys. **72**, 621 (2000).

[14] C.U. Segre, N.E. Leyarovska, L.D. Chapman, W.M. Lavender, P.W. Plag, A.S. King, A.J. Kropf, B.A. Bunker, K.M. Kemner, P. Dutta, R.S. Duran, and J. Kaduk, in *Synchrotron Radiation Instrumentation: SRI99: Eleventh US National Conference*, edited by Piero Pianetta, John Arthur, and Sean Brennan, AIP Conf. Proc. No. 521 (AIP, New York, 2000).

[15] *X-ray Absorption*, edited by D.C. Koningsberger and R. Prins (Wiley, New York, 1988).

[16] A.L. Ankudinov, B. Ravel, J.J. Rehr, and S.D. Conradson, Phys. Rev. B **58**, 7565 (1998).

[17] E.A. Stern, M. Newville, B. Ravel, Y. Yacoby, and D. Haskel, Physica B **208&209**, 117 (1995).

[18] J.T. Miller, C.L. Marshall, and A.J. Kropf, J. Catal. **202**, 89-99 (2001).

[19] A. J. Kropf (unpublished).

[20] H. Hotop and W.C. Lineberger, J. Phys. Chem. Ref. Data **4**, 539 (1975); R.J. Zollweg, J. Chem. Phys. **50**, 4251 (1969).

[21] In the framework of the more vaguely defined *electronegativity* concept, Li is expected to be a better electron donor than In; however, the concept of electronegativity is defined for molecules and not applicable for crystals. For values for elemental electronegativities, see, e.g., A.L. Allred and E.G. Rochow, J. Inorg. Nucl. Chem. **5**, 264 (1958)

[22] P. Villars and L.D. Calvert, *Pearson's Handbook of Cyrstallographic Data for Intermetallic Phases* (ASM International, Materials Park, OH, 1991), Vol. 4; G. Brauer and E. Zintl, Z. Phys. Chem. Abt. B **37**, 323 (1937).

[23] K.C. Hewitt, L.Y. Beaulieu, and J.R. Dahn, J. Electrochem. Soc. **148**, A402 (2001).